Hindawi Publishing Corporation
International Journal of Photoenergy
Volume 2012, Article ID 169829, 16 pages
doi:10.1155/2012/169829

Review Article

Crystal Growth Behaviors of Silicon during Melt Growth Processes

Kozo Fujiwara

Institute for Materials Research (IMR), Tohoku University, Katahira 2-1-1, Aoba-ku, Sendai 980-8577, Japan

Correspondence should be addressed to Kozo Fujiwara, kozo@imr.tohoku.ac.jp

Received 31 August 2011; Accepted 29 December 2011

Academic Editor: Teh Tan

It is imperative to improve the crystal quality of Si multicrystal ingots grown by casting because they are widely used for solar cells in the present and will probably expand their use in the future. Fine control of macro- and microstructures, grain size, grain orientation, grain boundaries, dislocation/subgrain boundaries, and impurities, in a Si multicrystal ingot, is therefore necessary. Understanding crystal growth mechanisms in melt growth processes is thus crucial for developing a good technology for producing high-quality Si multicrystal ingots for solar cells. In this review, crystal growth mechanisms involving the morphological transformation of the crystal-melt interface, grain boundary formation, parallel-twin formation, and faceted dendrite growth are discussed on the basis of the experimental results of in situ observations.

1. Introduction

The expectations for solar cells have been increasing yearly toward solving energy and environmental problems worldwide. The Si multicrystal (mc-Si) is one of the most important materials along with the Si single crystal (sc-Si) for the substrate of solar cells in the future although other materials are being developed. The crystal structure of an mc-Si ingot obtained by casting based on a unidirectional growth technique is markedly different from that of sc-Si, as illustrated by the formation of grain boundaries and the distribution of crystallographic orientations, which prevent the realization of high-efficiency solar cells. Various types of defect included in an mc-Si ingot, such as grain boundaries, dislocations, sub-grain boundaries, and metallic impurities, affect the properties of solar cells. Therefore, there is increasing importance to control the macro- and microstructures of mc-Si ingots. In recent years, various new methods for controlling the macro- and microstructures have been presented, which focus on controlling the nucleation or crystal growth mechanism in the earlier stage of casting. Dendritic casting is a method in which seed crystals are created from the melt during crystallization by inducing dendrite growth at the bottom of the crucible [1–3]. Seeded casting is a method in which prearranged seed crystals are set at the bottom of a crucible before crystallization, which initiates from seed crystals [4–6]. Other methods have been proposed, in which the nucleation site is controlled by controlling the cooling area in the initial stage of casting [7–9]. Many studies to establish such technologies for obtaining high-quality mc-Si ingots have been continuously performed on all these methods. In this review, such technologies for mc-Si ingot growth will not be discussed; only the melt growth mechanisms of Si will be discussed because fundamental understanding of crystal growth mechanisms is crucial to developing all such technologies. The crystal growth phenomena during melt growth processes including the morphological transformation of crystal-melt interfaces, grain boundary formation, parallel-twin formation, and faceted dendrite growth will be discussed by providing a review of our recent studies.

2. Morphological Transformation of Crystal-Melt Interface

2.1. Crystal-Melt Interface during Unidirectional Growth. To control the morphology of the crystal-melt interface during unidirectional growth processes is crucial to obtaining high-quality crystals because it affects the macro- and microstructures and eventually the mechanical, optical, and electrical

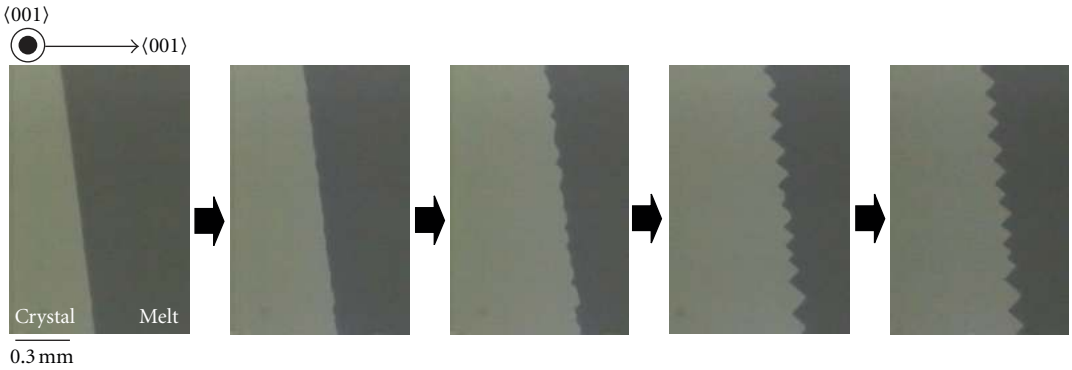

Figure 1: Morphological transformation of Si (100) crystal-melt interface moving at 162 μm/s [10].

properties of materials. It has been suggested that the generation of crystal defects, such as dislocations and twin boundaries, is related to the morphology of the crystal-melt interface [12–14]. The segregation of impurities is also dependent on the interfacial morphology [15]. According to Jackson's theory [16, 17], only the crystal-melt interfaces of Si {111} planes, called facet planes, are atomically smooth; other crystallographic planes are atomically rough. Because the {111} planes have the lowest surface energy [18], a zigzag-faceted interface bounded by {111} planes is expected to form at the crystal-melt interface of rough planes. The crystal-melt interface was observed in recrystallization processes in Si thin films [19–28], and micron-sized zigzag facets at the Si (100) crystal-melt interface were observed. Molecular dynamics simulation showed the existence of atomic-scale zigzag facets at the Si (100) crystal-melt interface [29, 30]. Such a zigzag-faceted interface at the Si (100) crystal-melt interface was also observed in bulk samples [31, 32]. Therefore, as one possible formation mechanism of a zigzag-faceted interface, it was considered that atomic-scale facets are initially formed, which gradually enlarge to macroscopic facets during crystallization [26]. On the other hand, recently, the zigzag-facet formation at the Si (100), (112), (110), and (111) crystal-melt interfaces has been investigated by in situ observation [10, 11].

Figure 1 shows the Si (100) crystal-melt interface whose growth velocity was 162 μm/s [10]. In this experiment, a piece of Si (100) wafer was set between quartz plates inside the furnace to keep the surface of the Si melt flat during crystal growth. The morphology of the interface transformed from planar to zigzag facets during the growth. It was shown that a wavelike perturbation is introduced into a planar interface, the perturbation is amplified, and the zigzag facets are formed finally. A similar morphological transformation from planar to zigzag facets of the moving interface was observed at the Si (112) and (110) crystal-melt interfaces at higher growth velocities, as shown in Figure 2 [11]. On the other hand, when the growth velocity was lower, the planar interfaces were maintained throughout the crystallization, as shown in Figure 3. The critical growth velocity for the morphological transformation, V_c, was found to be 123 μm/s $< V_c <$ 147 μm/s, 107 μm/s $< V_c <$ 124 μm/s, and 102 μm/s $< V_c <$ 129 μm/s at the Si (100), Si (110), and Si (112) crystal-melt interfaces, respectively [10, 11]. In those experiments, the temperature gradient along the growth direction in the furnace was about 8 K/mm. It was found that the critical growth velocity was dependent on the temperature gradient in the furnace. When the temperature gradient was about 4 K/mm, the critical growth velocity of the Si (100) interface was 36 μm/s $< V_c <$ 100 μm/s [33]. Figure 4 shows isochrones of the interface of Si (100) and Si (110) when the planar interface transformed to a zigzag-faceted interface. It was shown that the wavelength of the wavy interface completely agreed with that of the zigzag-faceted interface. The perturbation was amplified with time, and one perturbation peak formed one zigzag facet peak. Here, it should be determined why the perturbation is amplified when the growth velocity is high, using stability arguments [34]. Tokairin et al. calculated the thermal field in the Si crystal and melt during crystallization along the growth direction at a constant growth velocity, before the zigzag facet formation [10]. Generally, a crystal-melt interface becomes unstable, leading to the amplification of the perturbation, when the temperature gradient at the interface is negative along the growth direction [35]. However, the temperature gradient in the furnace was positive in Figures 1–4. Therefore, it was considered that the latent heat of crystallization increases the temperature at the crystal-melt interface, and that the temperature gradient in the Si melt at the interface becomes negative when growth velocity is high, because the amount of generated latent heat per unit time increases with growth velocity. The thermal field of the Si crystal and melt, $T_{c,m}$, is governed by the partial differential equation [36]

$$\rho_{c,m}C_{\mathrm{Pc},m}\frac{\partial T_{c,m}}{\partial t} = -\rho_{c,m}C_{\mathrm{Pc},m}V\frac{\partial T_{c,m}}{\partial X} = K_{c,m}\frac{\partial^2 T_{c,m}}{\partial X^2} + \frac{2K_q}{l_q l_{\mathrm{Si}}}(Gx + T_i - T_{c,m}), \quad (1)$$

where $\rho_{c,m}C_{\mathrm{Pc},m}$, $k_{c,m}$, k_q, l_q, and l_{Si} are the heat capacity of the Si crystal and melt, the thermal conductivity of the Si crystal and melt, the thermal conductivity of the quartz plate, the thickness of the quartz plate, and the thickness

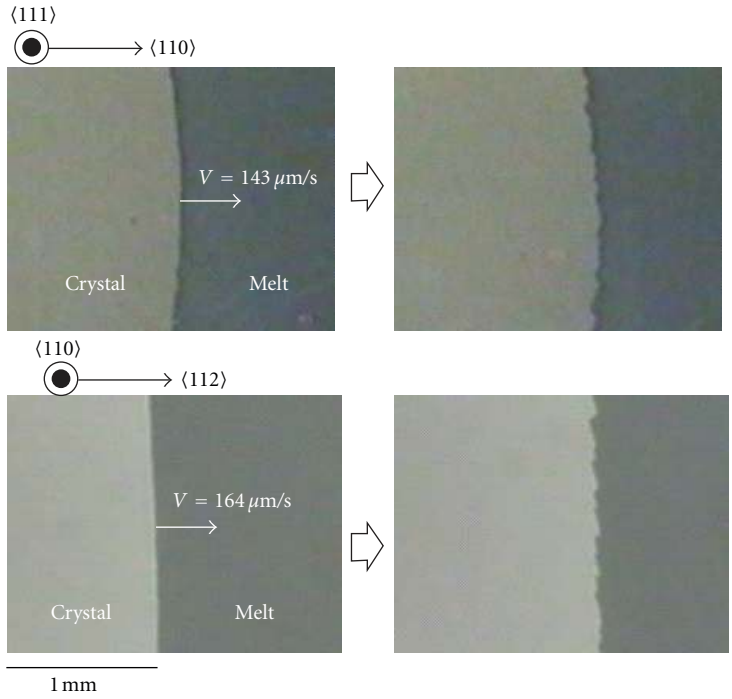

Figure 2: Morphological transformation of Si (110) and (112) crystal-melt interfaces at high growth velocities [11].

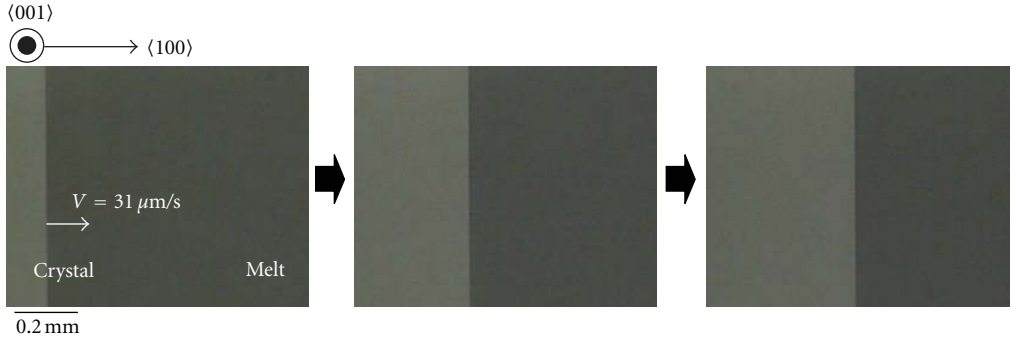

Figure 3: Morphology of Si (100) crystal-melt interface at low growth velocity [10].

of the Si, respectively. The origin of the coordinate is the crystal-melt interface, which moves with the growth velocity V. $Gx + T_i$ is the furnace temperature, where G is the temperature gradient in the furnace, and T_i is the furnace temperature at the interface. The first and second terms on the right-hand side of (1) come from the heat diffusion along the growth direction and the heat conduction between the Si crystal or melt and the furnace through the quartz plates, respectively. From the solution of (1), the thermal fields of the Si crystal and melt during crystal growth for various growth velocities were obtained, as shown in Figure 5 [10]. The physical properties of Si used were based on those indicated in [37], and l_q, l_{Si}, and G were based on experimental values. The temperature gradient in the Si melt at the interface changes from positive to negative as growth velocity increases. When the growth velocity is low, the temperature gradient is positive, and this means that the interface is stable and the planar interface is maintained. On the other hand, when the growth velocity exceeds its critical value, the temperature gradient in the Si melt at the interface changes from positive to negative, and thus the perturbation introduced into the planar interface is amplified, forming zigzag facets at high growth velocities.

Figure 6 shows the crystal-melt interface of the Si (111) plane growing at a high growth velocity of 200 μm/s. The Si (111) interface maintained a planar shape even at a high growth velocity although a negative temperature gradient should have been formed at the interface at such a high growth velocity. The difference in interface morphology between the (111) plane and the other planes could be explained by considering the anisotropy of growth velocity. The growth velocity along the ⟨111⟩ direction is the lowest. Moreover, the growth velocity on the Si (111) plane was more than 2 orders lower than that on the Si (100) plane at a given undercooling [38]. Thus, even though perturbation is introduced into the (111) planar interface, the morphology

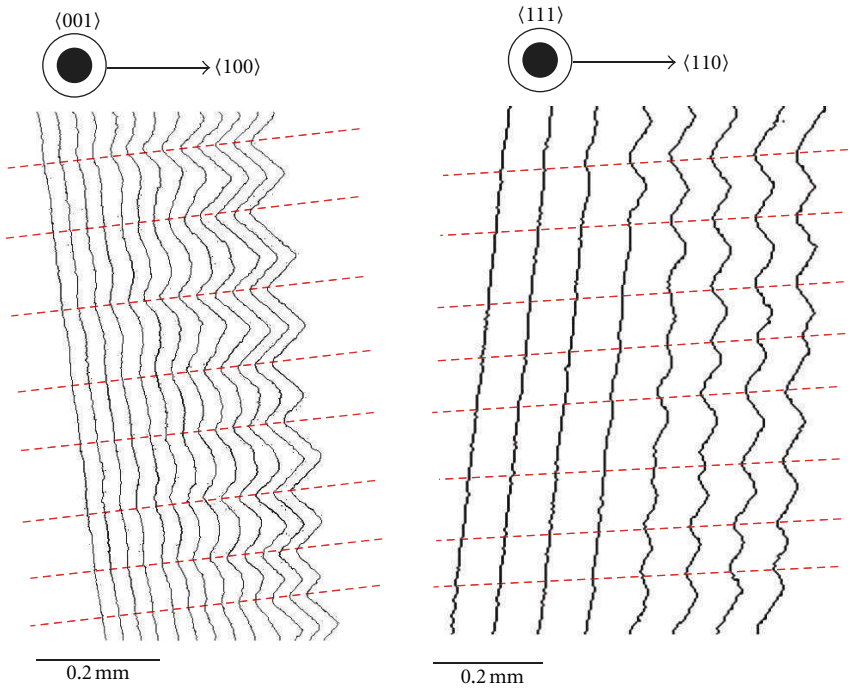

Figure 4: Isochrones of Si (100) and Si (110) interfaces when planar interface transformed to zigzag faceted interface [10].

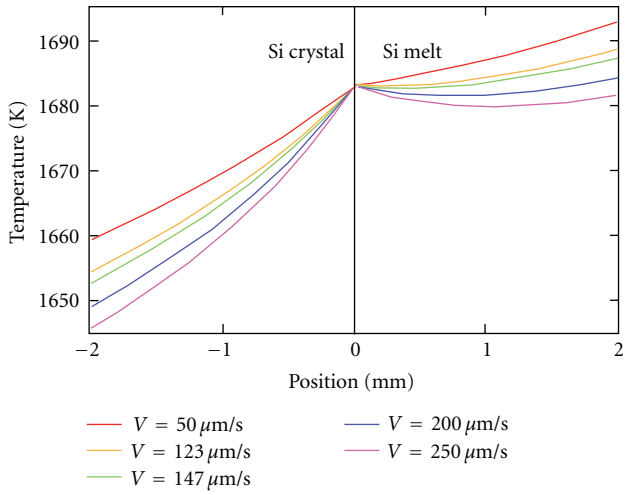

Figure 5: Calculated thermal fields of Si crystal and melt during crystallization for V = 50, 123, 147, 200, and 250 μm/s. $\rho_c C_{Pc}$ = 2.29 × 10^{-3} J/mm^3 K, $\rho_m C_{Pm}$ = 2.53 × 10^{-3} J/mm^3 K, k_c = 2.2 × 10^{-2} W/mm K, k_m = 5.4 × 10^{-2} W/mm K, k_q = 4.3 × 10^{-3} W/mm K, l_q = 1.0 mm, l_{Si} = 0.5 mm, G = 8 K/mm, ΔH = 4.122 J/mm^3, and T_{mp} = 1683 K. l_q, l_{Si}, and G are based on the experimental values, and the physical properties of Si used are based on those mentioned in [37]. The temperature gradient in the Si melt at the crystal-melt interface changed from positive to negative as V increased [10].

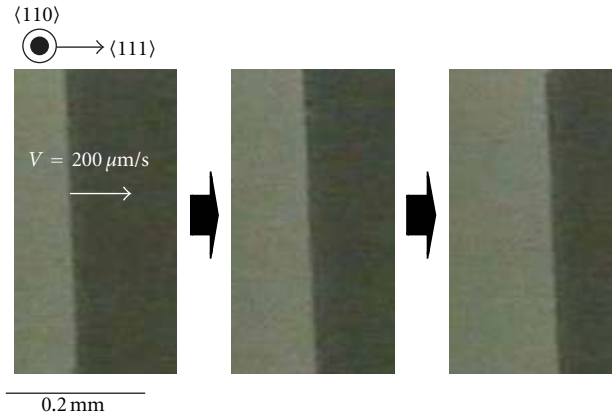

Figure 6: Typical image of the Si (111) crystal-melt interface during crystal growth [11].

of the interface remains planar owing to the faster growth in the lateral direction than in the ⟨111⟩ direction. For added consideration regarding the growth of the Si (111) interface, it was reported that the step-flow mode is stable up to an undercooling of 40 K by molecular dynamics simulation [39]. The step velocity at the (111) interface was found to be quite high because of the large step kinetic coefficients, that is, 0.29–0.79 m/sK. Such a high step velocity makes the interface planar in this growth mode.

It has been shown that the interface morphology is controlled by temperature gradient and growth velocity. When the zigzag facets are formed at the crystal-melt interface of rough planes during a unidirectional growth process of an mc-Si ingot by casting, the growth velocity difference between the rough planes and {111} facet planes becomes larger [32, 40]. When two crystal grains, the one has (100) interface and the other one has (111) interface, exist

side by side, the (100) grain with zigzag facets interface grows much faster than (111) grain with planar interface, and the (100) grain gradually occupies the space and becomes larger than (111) grain during the unidirectional growth. In such competitive growth process between the two crystal grains, the shape of the grain boundary between two crystal grains is also changing during the growth [32, 40]. The stress given to the grain boundary maybe increased with the shape change, which leads to increasing the defect generation, such as dislocations or twin boundaries, at the grain boundary. Moreover, when the zigzag facets are formed at the crystal-melt interface of rough planes during a unidirectional growth process, the impurities segregate at the valleys of zigzag facets, which lead to in-plane inhomogeneity in an ingot. Those phenomena seem to affect the quality of an mc-Si ingot in an adverse way. On the other hand, Si-faceted dendrites easily grow from a zigzag facets interface [12]. In the dendritic casting, faceted dendrites are promoted to grow along the bottom of the crucible in the earlier stage of casting [1]. In this method, the growth condition to form the zigzag facets interface should be selected to initiate the dendrite growth in the initial stage of casting, which leads to the formation of large-size grains at the bottom of the ingot. Thus, we should carefully control the growth mechanism during casting for obtaining high-quality mc-Si ingots.

2.2. Growth Kinetics in Melt Growth of Silicon. In the previous section, the morphological transformation of crystal-melt interfaces for different orientations was shown. Those phenomena observed at crystal-melt interface depend on the anisotropy of crystal-melt interfacial energy, which governs the growth kinetics and growth modes. It is well known that Si (111) is a facet plane, which means that the surface of crystal-melt interface is atomically smooth, and other planes are atomically rough. Therefore, the growth kinetics in melt growth processes seems to be different between the (111) plane and other planes. In general, the growth on the (111) facet plane is discussed by a 2D nucleation mode, and that of rough planes are discussed by a normal growth mode [38]. The normal growth velocity, V_n, on Si rough plane is expressed as $V_n = \beta_{\text{rough}} \Delta T$, where β_{rough} and ΔT are the kinetic coefficient for rough plane and undercooling at the crystal-melt interface, respectively. The value of the kinetic coefficient for Si (100) rough plane has been derived by computations as approximately 0.1 m/(sK) [38, 39]. Thus, the growth velocity on Si (100) rough plane linearly increases with increasing the amount of undercooling. On the other hand, the growth velocity on a Si (111) facet plane increases exponentially with undercooling in a 2D nucleation growth mode [38, 42]. Therefore, the growth velocity on a facet plane seems to be much smaller than that of the rough plane at a low undercooling. However, direct evidences by experiments for the growth kinetics in melt growth processes have been very limited comparing with those in the solution growth or the vapor growth. Thus, a more detailed discussion of the growth mode should be reserved for future works. The growth mode on a Si (111) facet plane has been well summarized in [42].

2.3. Crystal-Melt Interface at the Grain Boundary Formation. In mc-Si grown by a casting, grain boundaries are one of the main factors governing the mechanical, optical, and electrical properties. For instance, some of the grain boundaries inhibit the increase in the energy conversion efficiency of solar cells because they act as recombination centers of photocarriers. Therefore, the relationships between grain boundary properties and electrical activity have been extensively investigated [44–51]. Moreover, a $\{111\} \sum 3$ grain boundary, which is usually straight, is electrically inactive, but other CSL (coincidence site lattice) boundaries or random grain boundaries, which are straight, wavy or curved, are electrically active. Grain boundary structures are also investigated by transmission electron microscopy [52–54] or computer simulation [55–57]. Almost all studies of grain boundaries in Si have been performed after crystallization. Here, the crystal growth behaviors in grain boundary formation during crystallization from Si melt are shown.

Figure 7(a) shows the crystal growth behavior when two crystals converge during the crystallization process [41]. Most of the crystal-melt interface between the two crystals is linear, which suggests that the growth direction vertical to those interfaces is ⟨111⟩. In the underlying crystal, a sharp triangular corner is observed at the right edge of the interface when there is sufficient distance between the two growing crystals. This difference in interfacial shape is due to the difference in the growth direction owing to the existence of a grain boundary at the location marked by a red arrow in Figure 7(a). The sharp corner gradually flattens as the two crystals become approach each other. Figure 7(b) shows the result of crystallographic orientation analysis after crystallization determined by the electron backscattering diffraction pattern (EBSP) method [41]. The directions vertical to the grain boundary are shown in color using the inverse pole figure triangle. A linear grain boundary was formed corresponding to the shape of crystal-melt interfaces just before grain boundary formation. It is found that the growth directions vertical to the linear growing interfaces were ⟨111⟩ (shown in blue), and that the growth direction with a sharp-cornered interface in the underlying crystal was ⟨100⟩ (shown in red). Grain boundary characteristics are also indicated by colored lines in Figure 7(b). The grain boundary characteristic differs depending on location. A $(111) \sum 3$ grain boundary, shown by a red line, is formed where {111} facet planes impinge on each other. On the other hand, a random grain boundary, shown by a black line, is formed at a location where the shape transition of the growing interface occurs just before grain boundary formation. Figure 8(a) shows isochrones of the position of the growing interfaces at 1/3 s intervals for the sample shown in Figure 7, and Figure 8(b) shows the *t-x* plot of the growing interface at the two parts marked by the red and blue lines on the isochrones [41]. The color of dots in Figure 8(b) corresponds to the line color in Figure 8(a). The initial point of the shape transition of the interface is indicated in Figure 8(b). It is shown that the growth velocity of the growing interfaces, the gradient of the *t-x* curve, decreases from this point. This means that the amount of undercooling in front of the growing interface decreased and the melt temperature in

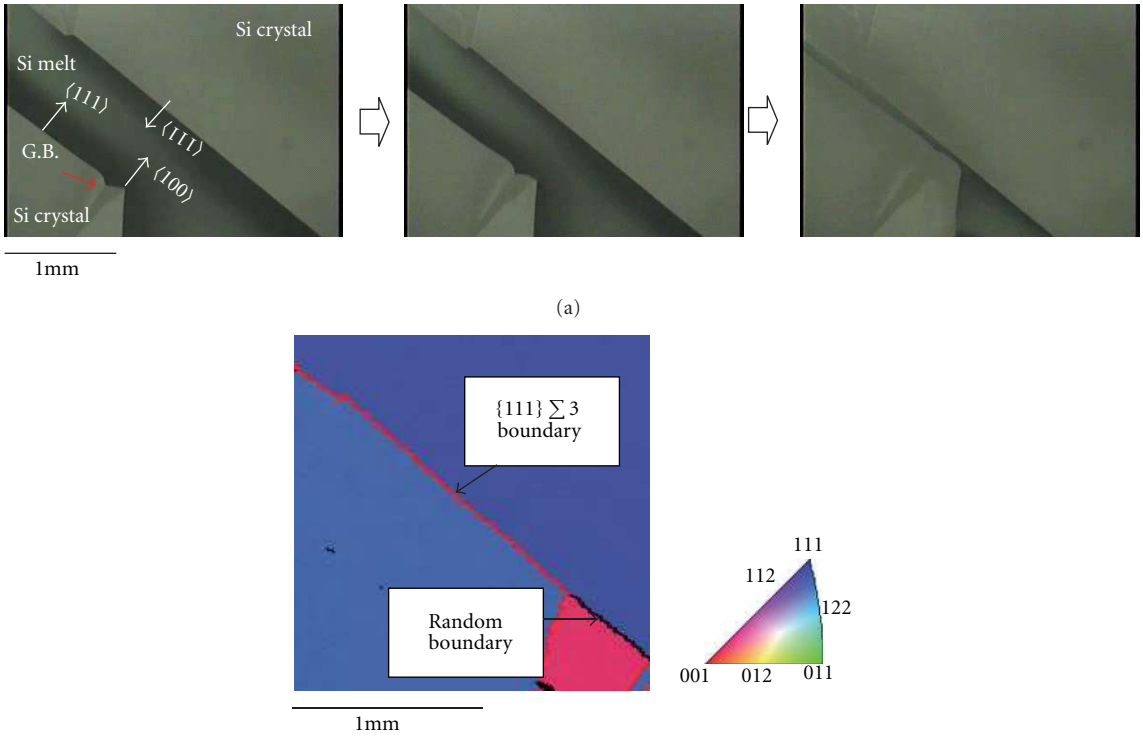

FIGURE 7: (a) Growth behavior of two Si crystals when they meet during crystallization. In the underlying crystal, the shapes of the growing interface are different on both sides of the grain boundary indicated by the arrow [41]. (b) Result of EBSP analysis of region observed in (a). The orientation vertical to the grain boundary is shown in color using the inverse pole figure triangle. The grain boundary is also shown in color in accordance with the grain boundary characteristics [41].

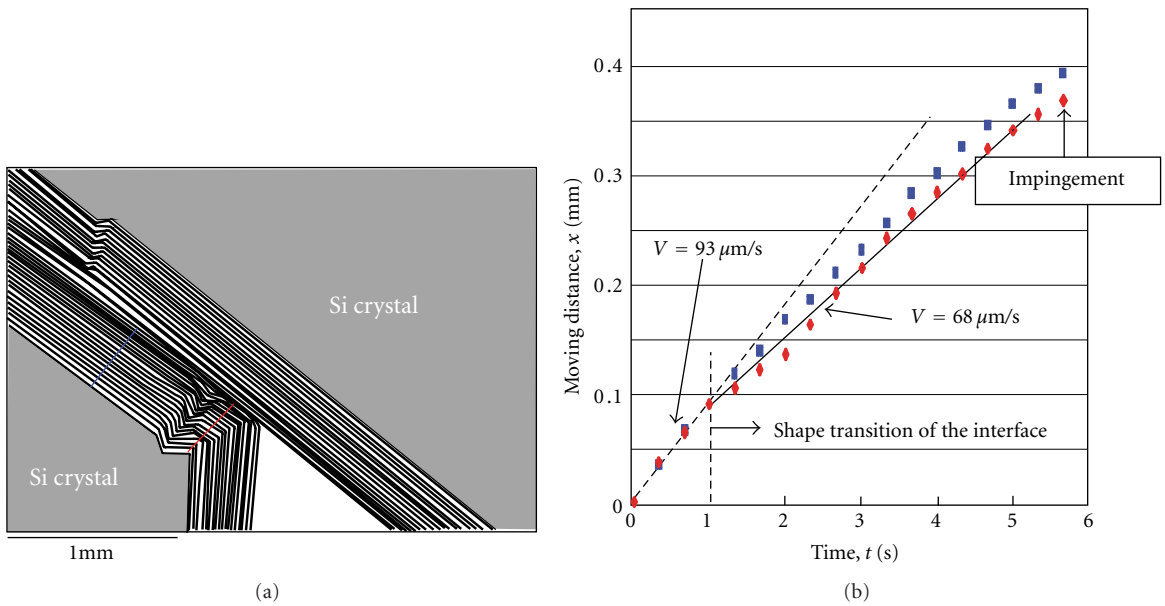

FIGURE 8: (a) Isochrones of positions of growing interface at 1/3 s intervals for sample shown in Figure 7 [41]. (b) *t*-*x* plot of moving interface for two parts shown by red and blue lines across isochrones in (a). The color of dots corresponds to the color of the lines in (a). The moving velocity of the interface is lower from the initiation point of the interface shape transition [41].

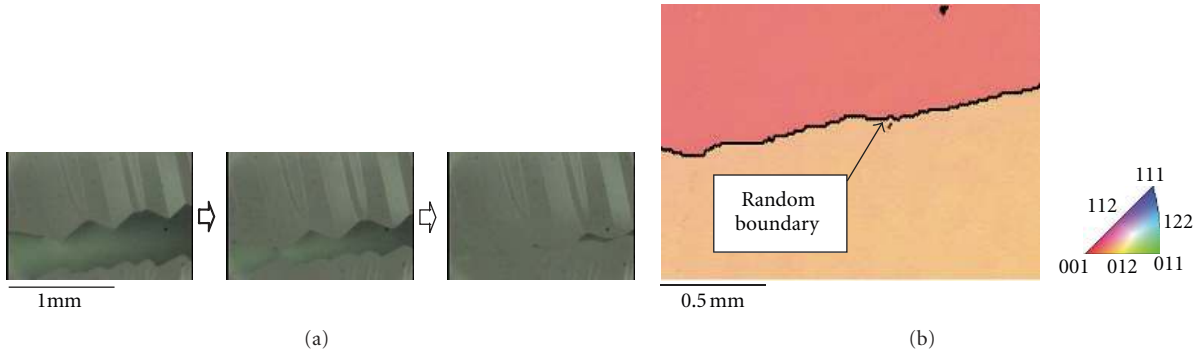

Figure 9: (a) Growth behavior of two Si crystals with zigzag-faceted interfaces [41]. It is observed that the sharp corners on the faceted interfaces gradually disappear as the crystals grow. (b) Result of EBSP analysis of the sample shown in (a) [41]. The growth direction vertical to the line indicated in (b) is shown in color.

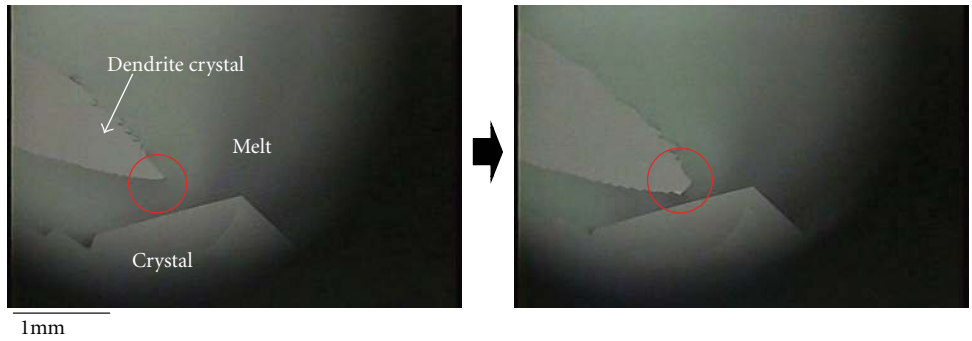

Figure 10: Growth behavior of faceted dendrite at grain boundary formation. The tip of the dendrite becomes flat during growth.

front of the growing interface increased. We explained this phenomenon by considering the thermal fields in front of the growing interface. When a crystal is growing from the melt, the heat of crystallization is released. The heat of crystallization can be taken away through the melt and/or crystal [58] when the two crystals are sufficiently separated. However, as the distance between two crystals becomes smaller, thermal fields in front of the two growing crystals overlap and the heat of crystallization cannot be taken away; then the temperature between the two crystals increases. This leads to the reduction in the growth velocity at the tip of the corner on the growing interface, and, as a result, the shape of the interface becomes flat. Figure 9(a) shows the growth behavior of the two crystals with zigzag-faceted interfaces [41]. Although the distance between the two crystals is large, well-developed {111} facet planes appear on the growth surfaces, and, thus, sharp corners are formed. As the distance between the two crystals becomes smaller, the shape transition of the growing interface is observed. The sharp corners on the interfaces gradually disappear, and wavy interfaces are formed. Just at impingement, the shape of the interfaces becomes more linear. This behavior of the growing interface is similar to that observed in Figure 7. Figure 9(b) shows the result of orientation analysis. The grain boundary was wavy owing to the shape transition of the growing interface, and a random grain boundary was formed [41]. The results in Figure 7 to Figure 9 show that the grain boundary shape and grain boundary characteristics are dependent on the behavior of the growing interface before impingement, which, in turn, strongly depends on the shape of the faceted interface. Figure 10 shows the growth behavior of the dendrite at the grain boundary formation. The tip of the dendrite is narrow and sharp when the distance between the two crystals is large. As the distance between the two crystals becomes smaller, the tip of the dendrite becomes wider and flatter. To continue the dendrite growth, sufficient undercooling, that is, more than 10 K, is necessary [12]. When the distance between the two crystals becomes smaller, melt temperature seems to increase owing to the overlapping thermal fields in front of the crystal-melt interfaces, as explained before, and then the dendrite growth cannot continue; thus, the tip of the dendrite is flattened.

3. Parallel-Twin Formation

In mc-Si ingots, twin boundaries are often observed at a high density [59]. The twin boundary formation energy is very low [60, 61], and some origins of twin boundary formation have been reported [16, 62–64]. Figure 11 shows an mc-Si wafer (left) and a faceted dendrite crystal examined by EBSP analysis (right). Most straight lines observed in the mc-Si wafer and the red lines at the center of the dendrite by EBSP analysis are twin boundaries. It is observed that at least two twin boundaries often exist parallel to each other, with a

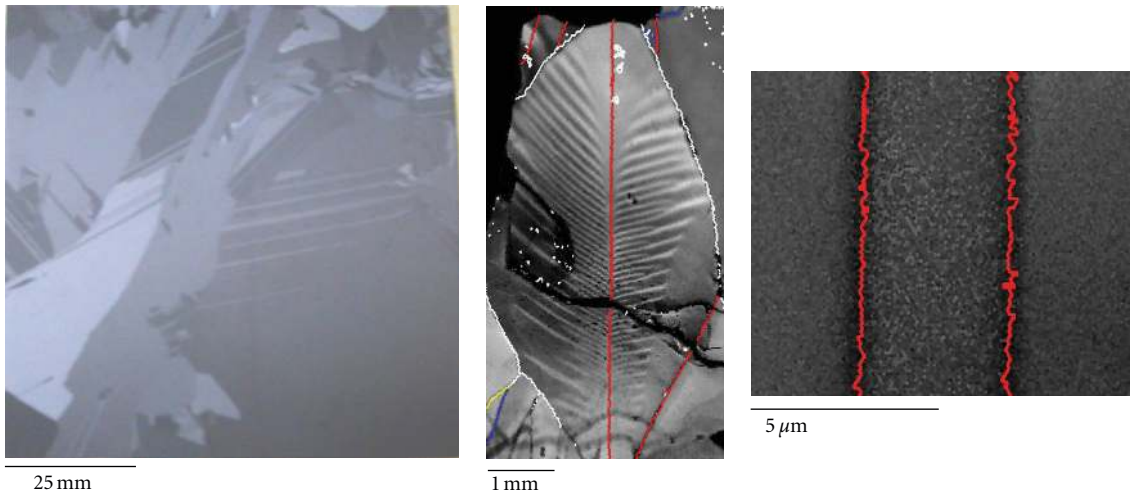

Figure 11: Mc-Si wafer (left) and faceted dendrite crystal examined by EBSP analysis (right) [43].

narrow spacing. Here, the parallel-twin formation, which is related to the faceted dendrite growth, is discussed.

The fundamental study of faceted dendrite growth has had a long history since the first report by Billig [65]. It has been shown that more than two parallel twins exist at the center of a faceted dendrite [65–69]. There have been some discussions concerning when and/or where a twin boundary is formed, that is, whether a nucleus originally contains a twin boundary [70] or whether a twin is formed after nucleation [71]. There was a report that twin boundaries are generated from a normal grain boundary during directional growth [72]. It has also been reported that parallel twins can form at (111) microfacets at a crystal-melt interface [43]. Pohl et al. studied this issue by classical molecular dynamics simulation [13]. In their simulations, parallel twin formation at the normal grain boundary was observed, but that at microfacets on a crystal-melt interface was not observed.

Figure 12 shows the growth behavior of a faceted dendrite grown from a crystal-melt interface. In this experiment, the crystal growth was initiated from a Si single-crystal seed. A faceted dendrite always appears following the zigzag facet formation on a crystal-melt interface during unidirectional growth. Figure 13 shows the result of the EBSP analysis of the faceted dendrite after crystallization. The EBSP analysis was performed at the origin of the dendrite growth. The direction along the dendrite growth was colored using the inverse pole figure triangle. $\sum 3$ grain boundaries were indicated by red lines, and other grain boundaries were labeled by black lines if they existed in the crystal. It was found that no grain boundaries without twin boundaries related to the dendrite growth existed in the crystal. This suggests that the grain boundary is not always necessary for twin boundary formation. To explain the experimental result, it should be considered that the twin boundary is formed on microfacets at the crystal-melt interface. Figure 14 schematically shows a model for generating parallel twins at the crystal-melt interface

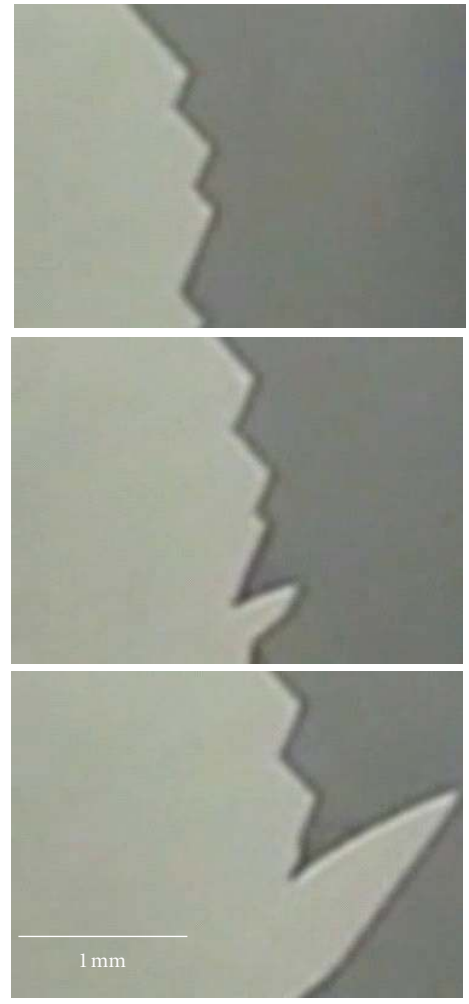

Figure 12: Growth behavior of faceted dendrite grown from crystal-melt interface.

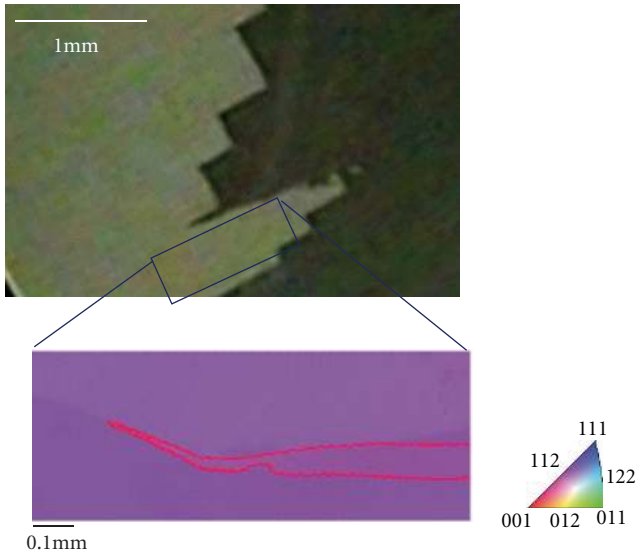

Figure 13: Result of EBSP analysis of faceted dendrite after crystallization. The EBSP analysis was performed at the origin of dendrite growth. The direction along the dendrite growth was shown in color using the inverse pole figure triangle. $\sum 3$ grain boundaries were indicated by red lines, and other grain boundaries were indicated by black lines when they existed in the crystal.

[43]. The formation of a zigzag-faceted interface bounded by {111} planes was discussed in Section 2.1. The shape of the faceted interface is dependent on crystal growth orientation, and crystal growth is always promoted on {111} facet planes at the zigzag-faceted interface. When an atom attaches to a facet plane with a twin relationship, a layer that maintains the twin relationship is formed on the facet plane after lateral growth, and then one twin boundary is generated on the layer, as shown in Figure 14(b). The crystal continuously grows in the lateral-growth mode on the {111} plane (Figure 14(c)), and then another twin boundary forms parallel to the previous twin boundary, as shown in Figure 14(d). In this model, the formation of parallel twin boundaries is ensured when one twin boundary is formed on a facet plane at the zigzag-faceted interface. When the undercooling of the melt is sufficient, a faceted dendrite grows from the parallel twin boundaries.

4. Faceted Dendrite Growth

Dendritic growth is a widespread phenomenon that appears during crystallization from a liquid or vapor phase in almost all types of materials containing metals, semiconductors, oxides, and organic materials. Dendrites of faceted materials, so-called "faceted dendrites," which are distinguished from those of nonfaceted materials in metals and alloys, were discovered in the 1950s [65]. It is known that the surface of a dendrite is bounded by {111} habit planes, and at least two parallel twin boundaries exist at the center of the dendrite [65–69]. Moreover, the preferential growth directions of Si-faceted dendrites are ⟨112⟩ and ⟨110⟩ [69], and the growth rate of faceted dendrites is higher than that of equiaxed grains. Such features can be applied in technologies for growing thin Si ribbon crystals [76, 77] and mc-Si ingots [1–3] for solar cells. The growth model of faceted dendrites preferentially grown in the ⟨112⟩ direction, hereafter referred to as ⟨112⟩ dendrites, was first proposed in 1960 by Hamilton and Seidensticker [67]. Recently, the growth model has been modified to apply to an actual growth based on experimental evidence by in situ observation of the growth behavior of ⟨112⟩ dendrites [74]. It was also shown that the modified model is adequate to explain the growth behavior of ⟨110⟩ dendrites [73].

Figure 15 shows a ⟨110⟩ dendrite and a ⟨112⟩ dendrite growing from a portion of a faceted crystal-melt interface. In both dendrites, parallel twins exist parallel to the {111} surface. The shape of the tip of the growing dendrite is markedly different between the ⟨110⟩ and ⟨112⟩ dendrites. Although the tip of the ⟨112⟩ dendrite becomes wider during growth, that of the ⟨110⟩ dendrite remains narrow during growth. Figure 16 shows the growth process of the ⟨112⟩ dendrite. It was found that triangular corners with an angle of 60° were formed at the tip of the dendrite and that the direction of the corners alternately changed from outward to forward in the direction of growth [74].

The modified growth model of the ⟨112⟩ dendrite based on experimental evidence is shown in Figure 17 [74]. Figure 17(a) shows the equilibrium form of the Si crystal with two parallel twins. The crystal is bounded by {111} habit planes, and parallel twin planes exist parallel to the ⟨111⟩ upper surface. In the explanation, the twins are distinguished by labeling them twin_1 and twin_2. A reentrant corner with an external angle of 141° (type I) appears at the growth surface only at twin_1 when the dendrite is growing in one direction. Nucleation more readily occurs at the reentrant corner than at {111} flat surfaces [69, 73, 74, 78–80], and thus the rapid growth occurs there. In this mechanism, it is considered that a triangular corner with an angle of 60° is formed at the growth tip of a dendrite owing to the rapid growth at the reentrant type I corner, as shown in Figure 17(b). This is the major difference from the previous growth mechanism of the ⟨112⟩ dendrite presented by Hamilton and Seidensticker [67]. In their explanation, it was considered that the formation of a triangular corner disturbs the continuous growth of a dendrite because the reentrant type I corner disappears. However, the formation of a triangular corner at the tip of the ⟨112⟩ dendrite is observed in Figure 16 by in situ observation [74]. Crystal growth can continue on the {111} flat surface although the rapid growth is inhibited owing to the disappearance of the type I corner (Figures 17(b)-17(c)). After the propagation of the crystal, two new type I corners are formed on the growth surface at twin_2 (Figure 17(c)). Thus, rapid growth occurs there again, and triangular corners with an angle of 60° are formed in the same manner as before (Figure 17(d)). Crystal growth is promoted on the {111} flat surface, leading to the formation of a new reentrant type I corner at twin_1 (Figure 17(e)), and the rapid growth occurs again (Figure 17(f)). A faceted dendrite continues to grow by the repetition of the same processes. In this

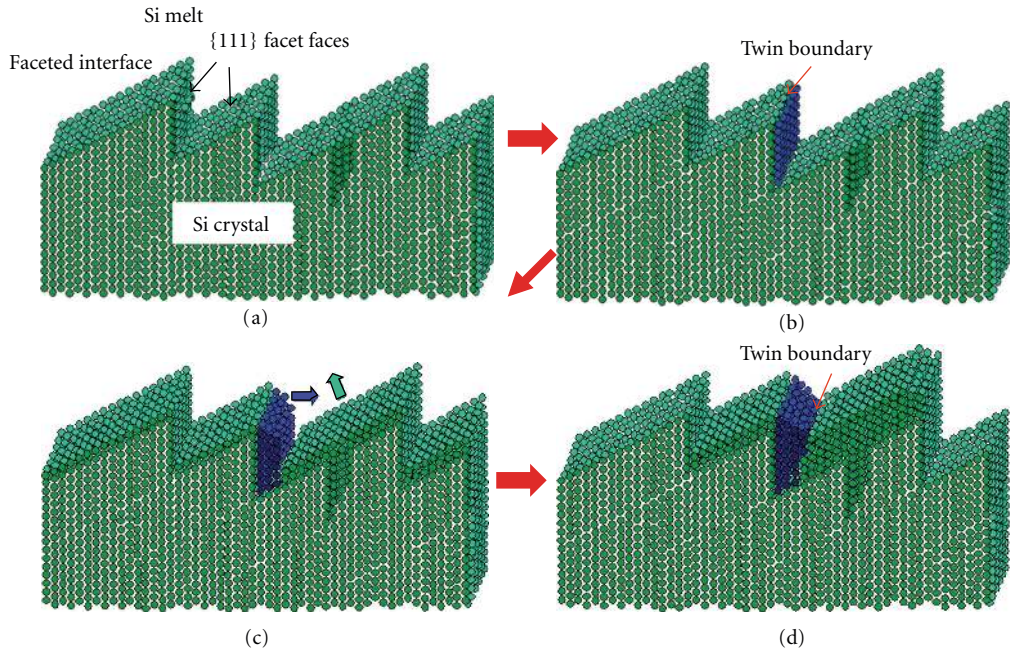

Figure 14: Model of parallel-twin formation at crystal-melt interface during crystal growth from Si melt. When a twin boundary is accidentally formed on a {111} facet plane, another twin boundary is formed parallel to the first twin after lateral growth is promoted [43].

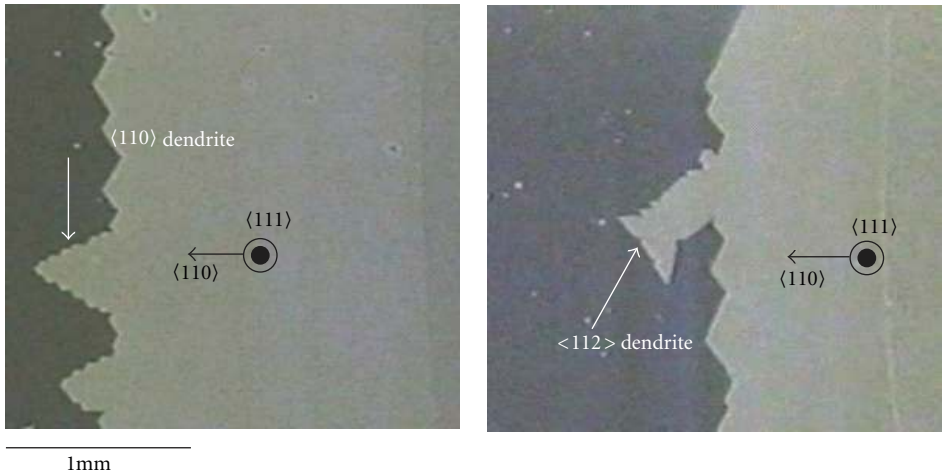

Figure 15: Growth shape of Si ⟨112⟩ and ⟨110⟩ faceted dendrites [73].

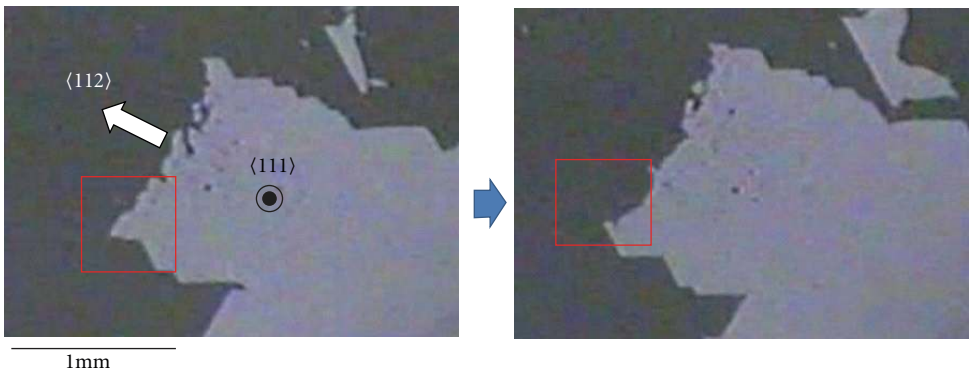

Figure 16: Growth behavior of Si ⟨112⟩ faceted dendrite observed perpendicular to {111} twins. Triangular corners of angle 60° are formed at the growth, tip and the direction of the corner changes with growth [74].

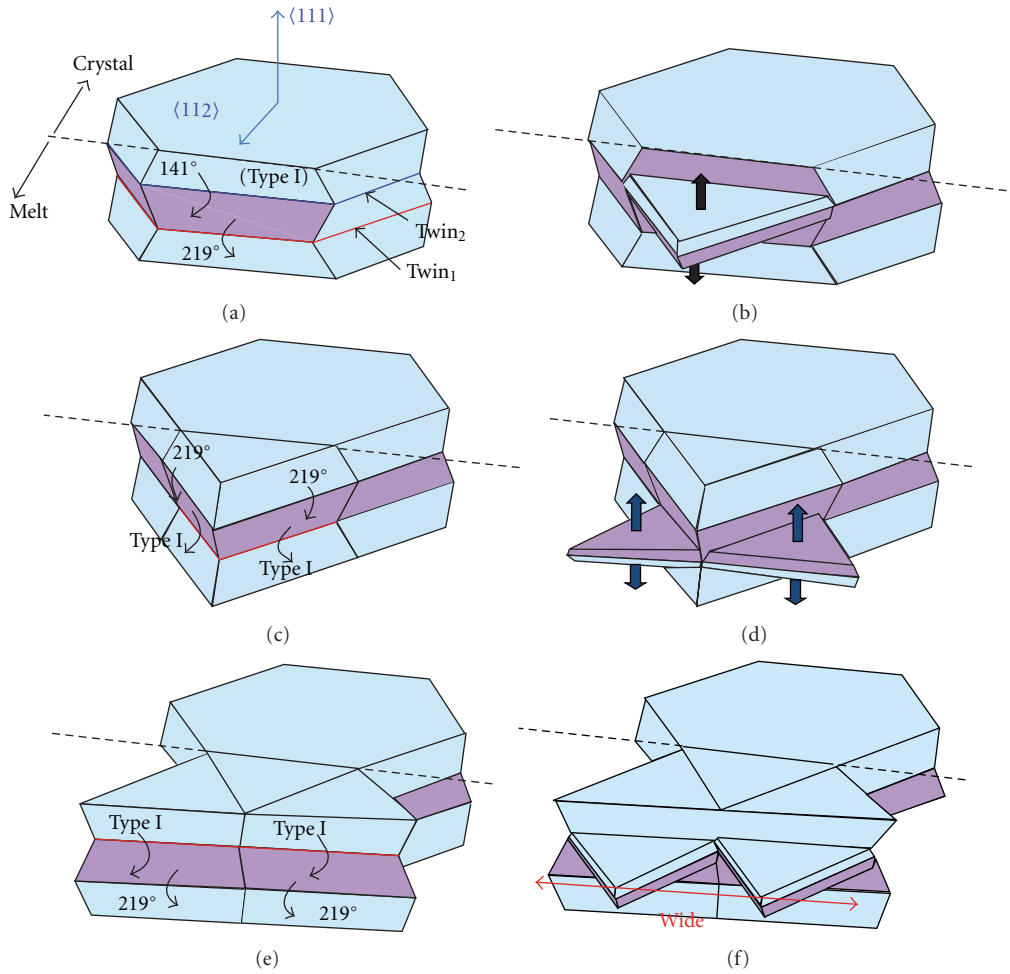

FIGURE 17: Schematic images of growth of Si ⟨112⟩ dendrite [73, 74]. (a) Equilibrium form of a crystal with two twins, which is bounded by {111} habit planes. It is considered that the crystal grows only in the ⟨112⟩ direction for simplicity. A reentrant corner of 141° angle (type I) appears at the growth surface only at twin$_1$. (b) A triangular corner is formed owing to the rapid growth at the type I corner at twin$_1$. (c) Crystal growth can continue on the {111} flat surface although the rapid growth is inhibited because of the disappearance of the type I corner. When the triangular crystal propagates across twin$_2$, two new type I corners are formed at twin$_2$. (d) Rapid growth occurs at the two type I corners again, and a triangular corner is formed. (e) After the propagation of the crystal, a type I corner is formed at twin$_1$. (f) Rapid growth occurs at a type I corner. A faceted dendrite continues to grow along the ⟨112⟩ direction by repeating the process from (b) to (f). The tip of the ⟨112⟩ dendrite becomes wider with crystal growth.

model, the tip of the ⟨112⟩ dendrite becomes wider during the growth.

Figure 18 shows the growth mechanism of a ⟨110⟩ dendrite [73]. Two parallel twins are also contained in this dendrite, and thus the initial shape of the crystal should be the same as that shown in Figure 17(a). This means that the elemental process for the growth of the ⟨110⟩ dendrite is the same as that of the ⟨112⟩ dendrite. It is found that type I corners exist at both twin$_1$ and twin$_2$ on the growth surface (Figure 18(a)). This is the major difference from the case of the ⟨112⟩ dendrite, in which type I corners alternately appear at each twin. Rapid growth occurs at these type I corners (Figure 18(b)), leading to the formation of triangular corners. Although the rapid growth is inhibited after the formation of triangular corners, the crystal continuously grows on the {111} flat surface (Figures 18(b)-18(c)). When triangular crystals propagate across the other twin, two type I corners appear, and rapid growth occurs there again (Figures 18(c)-18(d)). When triangular crystals propagate across the other twin, two type I corners appear (Figure 18(e)). The tip of the dendrite remains narrow during crystal growth. Thus, the shapes of the ⟨112⟩ and ⟨110⟩ dendrites during growth are explained by the models shown in Figures 17 and 18.

The equation for the growth velocity of a ⟨112⟩ dendrite and a ⟨110⟩ dendrite is derived on the basis of the growth model shown in Figures 17 and 18 [75]. The growth velocities of both dendrites are, respectively, described as

$$V_{\langle 112\rangle} = \frac{h}{2\,(h/V_1 + d/V_2)} + V_2,$$
$$V_{\langle 110\rangle} = \frac{h}{\sqrt{3}\,(h/V_1 + d/V_2)} + V_2, \quad (2)$$

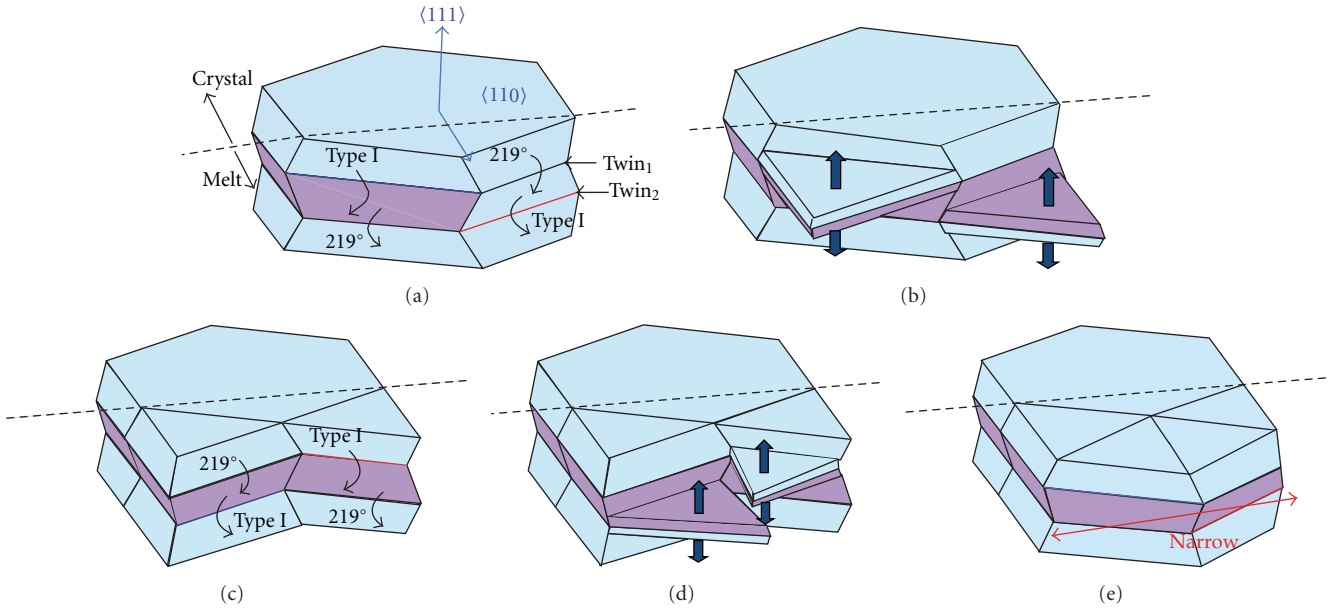

FIGURE 18: Schematic images of growth of Si ⟨110⟩ dendrite [73]. (a) Equilibrium form of crystal with two twins, which is similar to that shown in Figure 17(a). It is considered that the crystal grows only in the ⟨110⟩ direction. Reentrant type I corners appear at both twin_1 and twin_2. This is markedly different from the growth of the ⟨112⟩ dendrite. (b) Triangular corners are formed owing to the rapid growth at both twins. (c) Crystal growth can continue on the {111} flat surface. When triangular crystals propagate across another twin, two new type I corners are formed at both twins. (d) Rapid growth occurs at the two type I corners again, and a triangular corner is formed. (e) After the propagation of the triangular crystals, type I corners are formed at both twins. A faceted dendrite continues to grow along the ⟨110⟩ direction by repeating the process from (b) to (e). The tip of the ⟨110⟩ dendrite remains narrow during crystal growth.

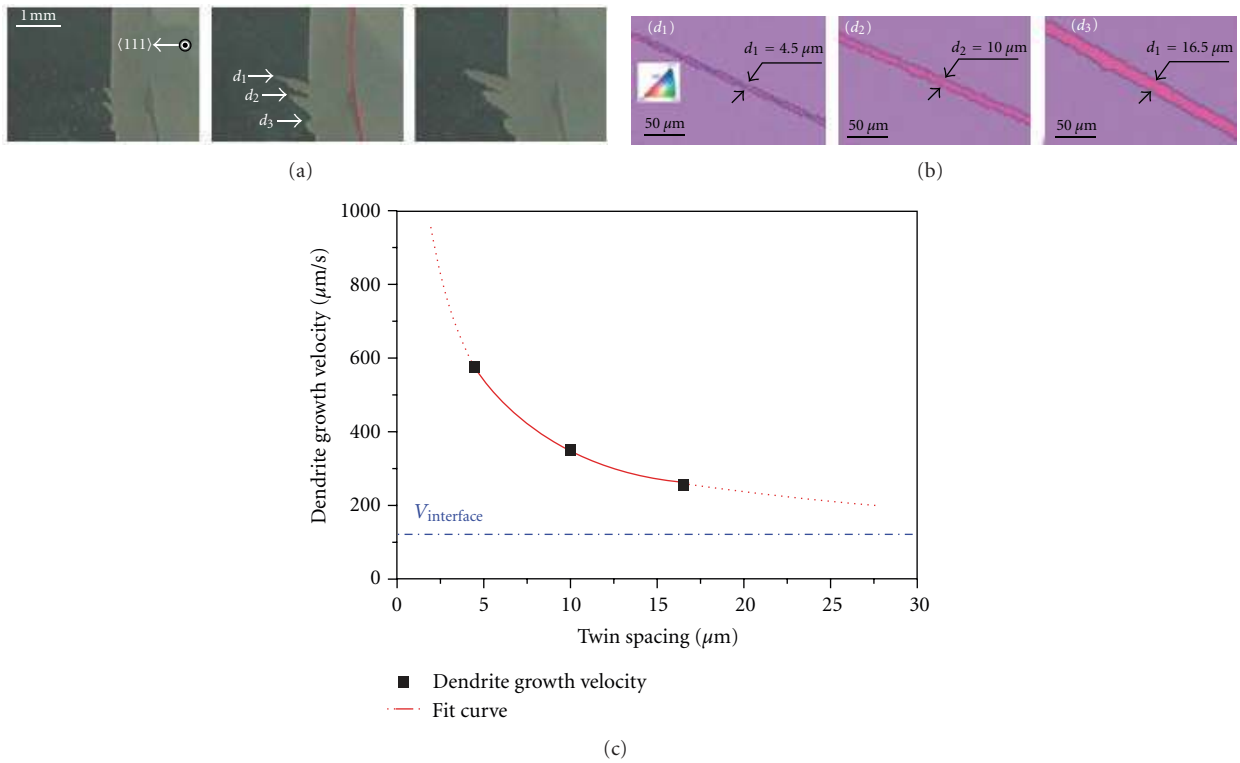

FIGURE 19: (a) Growth process of three dendrites (d1, d2, and d3) grown from same crystal-melt interface at same time [75]. (b) Parallel twins observed at center of d1, d2, and d3 by EBSP measurement. The average twin spacings in d1, d2, and d3 are 4.5 μm, 10 μm, and 16.5 μm, respectively [75]. (c) Dendrite growth velocity as function of twin spacing [75].

where h is the height of a triangular corner, d is the twin spacing, V_1 is the growth velocity at a type I corner, and V_2 is the growth velocity on the {111} plane. It is found that the growth velocity of a dendrite is inversely proportional to twin spacing. Figure 19(a) shows the growth of three dendrites (d1, d2, and d3) from the same crystal-melt interface at the same time [75]. The preferential growth direction of these three dendrites is ⟨110⟩. The growth velocities are clearly different among the three dendrites. Figure 19(b) shows the parallel twins observed at the center of d1, d2, and d3 by EBSP measurement. The average twin spacings in d1, d2, and d3 are 4.5 μm, 10 μm, and 16.5 μm, respectively. Dendrite growth velocity as a function of twin spacing is plotted in Figure 19(c). As twin spacing decreases, dendrite growth velocity nonlinearly increases. The equation above was used to fit the experimental results, as shown by the red line in Figure 19(c). It is found that the growth velocity of a dendrite eventually approaches a certain value as twin spacing increases to infinity. The dependence of the growth velocity of faceted dendrites on undercooling was also investigated [81]. Dendrite growth velocity increased linearly with increasing undercooling. It was also found that the relationship between dendrite growth velocity and undercooling is most sensitive to twin spacing [81].

5. Summary

Some crystal growth behaviors observed in melt growth processes were reviewed in this paper. Other significant issues not treated in this review include the dislocation/sub-grain-boundary formation [82–87] and impurity behavior [88–93] in crystal growth processes. For the complete understanding of crystal growth mechanisms and the control of the macro- and microstructures of mc-Si ingots, further data accumulation is required. It is expected that such ongoing studies will lead to the establishment of a technology for producing high-quality mc-Si ingots in the near future.

Acknowledgment

The author would like to acknowledge S. Uda and K. Nakajima for their fruitful discussions. This work was partially funded by the JST PRESTO Program and the Cabinet Office, Government of Japan through its "Funding Program for Next Generation World-Leading Researchers."

References

[1] K. Fujiwara, W. Pan, N. Usami et al., "Growth of structure-controlled polycrystalline silicon ingots for solar cells by casting," *Acta Materialia*, vol. 54, no. 12, pp. 3191–3197, 2006.

[2] K. Fujiwara, W. Pan, K. Sawada et al., "Directional growth method to obtain high quality polycrystalline silicon from its melt," *Journal of Crystal Growth*, vol. 292, no. 2, pp. 282–285, 2006.

[3] K. Nakajima, K. Kutsukake, K. Fujiwara, K. Morishita, and S. Ono, "Arrangement of dendrite crystals grown along the bottom of Si ingots using the dendritic casting method by controlling thermal conductivity under crucibles," *Journal of Crystal Growth*, vol. 319, no. 1, pp. 13–18, 2011.

[4] N. Stoddard, B. Wu, I. Witting et al., "Casting single crystal silicon: novel defect profiles from BP solar's mono2 wafers," *Diffusion and Defect Data Part B*, vol. 131–133, pp. 1–8, 2008.

[5] B. Wu and R. Clark, "Influence of inclusion on nucleation of silicon casting for photovoltaic (PV) application," *Journal of Crystal Growth*, vol. 318, no. 1, pp. 200–207, 2011.

[6] H. Zhang, L. Zheng, X. Ma, B. Zhao, C. Wang, and F. Xu, "Nucleation and bulk growth control for high efficiency silicon ingot casting," *Journal of Crystal Growth*, vol. 318, no. 1, pp. 283–287, 2011.

[7] T. Y. Wang, S. L. Hsu, C. C. Fei, K. M. Yei, W. C. Hsu, and C. W. Lan, "Grain control using spot cooling in multi-crystalline silicon crystal growth," *Journal of Crystal Growth*, vol. 311, no. 2, pp. 263–267, 2009.

[8] Y. Nose, I. Takahashi, W. Pan, N. Usami, K. Fujiwara, and K. Nakajima, "Floating cast method to realize high-quality Si bulk multicrystals for solar cells," *Journal of Crystal Growth*, vol. 311, no. 2, pp. 228–231, 2009.

[9] K. M. Yeh, C. K. Hseih, W. C. Hsu, and C. W. Lan, "High-quality multi-crystalline silicon growth for solar cells by grain-controlled directional solidification," *Progress in Photovoltaics: Research and Applications*, vol. 18, no. 4, pp. 265–271, 2010.

[10] M. Tokairin, K. Fujiwara, K. Kutsukake, N. Usami, and K. Nakajima, "Formation mechanism of a faceted interface: in situ observation of the Si(100) crystal-melt interface during crystal growth," *Physical Review B*, vol. 80, no. 17, Article ID 174108, 2009.

[11] K. Fujiwara, R. Gotoh, X. B. Yang, H. Koizumi, J. Nozawa, and S. Uda, "Morphological transformation of a crystal-melt interface during unidirectional growth of silicon," *Acta Materialia*, vol. 59, no. 11, pp. 4700–4708, 2011.

[12] K. Fujiwara, K. Maeda, N. Usami et al., "In situ observation of Si faceted dendrite growth from low-degree-of-undercooling melts," *Acta Materialia*, vol. 56, no. 11, pp. 2663–2668, 2008.

[13] J. Pohl, M. Müller, A. Seidl, and K. Albe, "Formation of parallel (1 1 1) twin boundaries in silicon growth from the melt explained by molecular dynamics simulations," *Journal of Crystal Growth*, vol. 312, no. 8, pp. 1411–1415, 2010.

[14] T. Duffar and A. Nadri, "On the twinning occurrence in bulk semiconductor crystal growth," *Scripta Materialia*, vol. 62, no. 12, pp. 955–960, 2010.

[15] K. A. Jackson, K. M. Beatty, and K. A. Gudgel, "An analytical model for non-equilibrium segregation during crystallization," *Journal of Crystal Growth*, vol. 271, no. 3-4, pp. 481–494, 2004.

[16] K. A. Jackson, *Liquid Metal and Solidification*, American Society for Metals, Cleveland, Ohio, USA, 1958.

[17] K. A. Jackson, "On the twinning occurrence in bulk semiconductor crystal growth," *Materials Science and Engineering*, vol. 65, no. 1, pp. 7–13, 1984.

[18] D. J. Eaglesham, A. E. White, L. C. Feldman, N. Moriya, and D. C. Jacobson, "Equilibrium shape of Si," *Physical Review Letters*, vol. 70, no. 11, pp. 1643–1646, 1993.

[19] M. W. Geis, H. I. Smith, B. Y. Tsaur, J. C. C. Fan, D. J. Silversmith, and R. W. Mountain, "Zone-melting recrystallization of Si films with a moveable-strip-heater oven," *Journal of the Electrochemical Society*, vol. 129, no. 12, pp. 2812–2818, 1982.

[20] M. W. Geis, H. I. Smith, D. J. Silversmith, R. W. Mountain, and C. V. Thomson, "Solidification-front modulation to entrain

subboundaries in zone-melting recrystallization of Si on SiO_2," *Journal of the Electrochemical Society*, vol. 130, no. 5, pp. 1178–1183, 1983.

[21] J. C. C. Fan, B. Y. Tsaur, and M. W. Geis, "Graphite-strip-heater zone-melting recrystallization of Si films," *Journal of Crystal Growth*, vol. 63, no. 3, pp. 453–483, 1983.

[22] E. H. Lee and G. A. Rozgonyi, "Modes of growth stability breakdown in the seeded crystallization of microzone-melted silicon on insulator," *Journal of Crystal Growth*, vol. 70, no. 1-2, pp. 223–229, 1984.

[23] L. Pfeiffer, S. Paine, G. H. Gilmer, W. van Saarloos, and K. W. West, "Pattern formation resulting from faceted growth in zone-melted thin films," *Physical Review Letters*, vol. 54, no. 17, pp. 1944–1947, 1985.

[24] D. Dutartre, M. Haond, and D. Bensahel, "Study of the solidification front of Si films in lamp zone melting controlled by patterning the underlying SiO_2," *Journal of Applied Physics*, vol. 59, no. 2, pp. 632–635, 1986.

[25] J. S. Im, H. Tomita, and C. V. Thompson, "Cellular and dendritic morphologies on stationary and moving liquid-solid interfaces in zone-melting recrystallization," *Applied Physics Letters*, vol. 51, no. 9, pp. 685–687, 1987.

[26] L. Pfeiffer, A. E. Gelman, K. A. Jackson, K. W. West, and J. L. Batstone, "Subboundary-free zone-melt recrystallization of thin-film silicon," *Applied Physics Letters*, vol. 51, no. 16, pp. 1256–1258, 1987.

[27] D. A. Williams, R. A. McMahon, and H. Ahmed, "Dynamic morphology of the nonequilibrium solid-melt interface in silicon," *Physical Review B*, vol. 39, no. 14, pp. 10467–10469, 1989.

[28] D. K. Shangguan and J. D. Hunt, "Dynamical study of the pattern formation of faceted cellular array growth," *Journal of Crystal Growth*, vol. 96, no. 4, pp. 856–870, 1989.

[29] U. Landman, W. D. Luedtke, R. N. Barnett et al., "Faceting at the silicon (100) crystal-melt interface: theory and experiment," *Physical Review Letters*, vol. 56, no. 2, pp. 155–158, 1986.

[30] U. Landman, W. D. Luedtke, M. W. Ribarsky, R. N. Barnett, and C. L. Cleveland, "Molecular-dynamics simulations of epitaxial crystal growth from the melt. I. Si(100)," *Physical Review B*, vol. 37, no. 9, pp. 4637–4646, 1988.

[31] K. Fujiwara, K. Nakajima, T. Ujihara et al., "In situ observations of crystal growth behavior of silicon melt," *Journal of Crystal Growth*, vol. 243, no. 2, pp. 275–282, 2002.

[32] K. Fujiwara, Y. Obinata, T. Ujihara, N. Usami, G. Sazaki, and K. Nakajima, "Grain growth behaviors of polycrystalline silicon during melt growth processes," *Journal of Crystal Growth*, vol. 266, no. 4, pp. 441–448, 2004.

[33] M. Tokairin, K. Fujiwara, K. Kutsukake, N. Usami, and K. Nakajima, "Formation mechanism of a faceted interface: in situ observation of the Si (100) crystal-melt interface during crystal growth," *Physical Review B*, vol. 80, no. 17, Article ID 174108, 2009.

[34] W. W. Mullins and R. F. Sekerka, "Stability of a planar interface during solidification of a dilute binary alloy," *Journal of Applied Physics*, vol. 35, no. 2, pp. 444–451, 1964.

[35] W. Kurz and D. J. Fisher, *Fundamentals of Solidification*, Trans Tech Publications, Dürnten, Switzerland, 4th revised edition, 1998.

[36] W. M. Rohsenow, J. P. Hartnett, and E. N. Ganic, *Handbook of Heat Transfer Fundamentals*, chapter 1, McGraw-Hill, New York, NY, USA, 2nd edition, 1985.

[37] K. W. Yi, H. T. Chung, H. W. Lee, and J. K. Yoon, "The effects of pulling rates on the shape of crystal/melt interface in Si single crystal growth by the Czochralski method," *Journal of Crystal Growth*, vol. 132, no. 3-4, pp. 451–460, 1993.

[38] K. M. Beatty and K. A. Jackson, "Monte Carlo modeling of silicon crystal growth," *Journal of Crystal Growth*, vol. 211, no. 1–4, pp. 13–17, 2000.

[39] D. Buta, M. Asta, and J. J. Hoyt, "Kinetic coefficient of steps at the Si(111) crystal-melt interface from molecular dynamics simulations," *Journal of Chemical Physics*, vol. 127, no. 7, Article ID 074703, 2007.

[40] P. Chen, Y. L. Tsai, and C. W. Lan, "Phase field modeling of growth competition of silicon grains," *Acta Materialia*, vol. 56, no. 15, pp. 4114–4122, 2008.

[41] K. Fujiwara, S. Tsumura, M. Tokairin et al., "Growth behavior of faceted Si crystals at grain boundary formation," *Journal of Crystal Growth*, vol. 312, no. 1, pp. 19–23, 2009.

[42] W. Miller, "Some remarks on the undercooling of the Si (1 1 1) facet and the "monte Carlo modeling of silicon crystal growth" by Kirk M. Beatty & Kenneth A. Jackson, J. Crystal Growth 211 (2000) 13," *Journal of Crystal Growth*, vol. 325, no. 1, pp. 101–103, 2011.

[43] K. Fujiwara, K. Maeda, N. Usami, G. Sazaki, Y. Nose, and K. Nakajima, "Formation mechanism of parallel twins related to Si-facetted dendrite growth," *Scripta Materialia*, vol. 57, no. 2, pp. 81–84, 2007.

[44] H. F. Mataré, "Carrier transport at grain boundaries in semiconductors," *Journal of Applied Physics*, vol. 56, no. 10, pp. 2605–2631, 1984.

[45] C. R. M. Grovenor, "Grain-boundaries in semiconductors," *Journal of Physics C*, vol. 18, no. 21, pp. 4079–4119, 1985.

[46] K. Yang, G. H. Schwuttke, and T. F. Ciszek, "Structural and electrical characterization of crystallographic defects in silicon ribbons," *Journal of Crystal Growth*, vol. 50, no. 1, pp. 301–310, 1980.

[47] A. Bary and G. Nouet, "Electrical activity of the first- and second-order twins and grain boundaries in silicon," *Journal of Applied Physics*, vol. 63, no. 2, pp. 435–438, 1988.

[48] R. Rizk, A. Ihlal, and X. Portier, "Evolution of electrical activity and structure of nickel precipitates with the treatment temperature of a Σ=25 silicon bicrystal," *Journal of Applied Physics*, vol. 77, no. 5, pp. 1875–1880, 1995.

[49] Z. J. Wang, S. Tsurekawa, K. Ikeda, T. Sekiguchi, and T. Watanabe, "Relationship between electrical activity and grain boundary structural configuration in polycrystalline silicon," *Interface Science*, vol. 7, no. 2, pp. 197–205, 1999.

[50] J. Chen, T. Sekiguchi, D. Yang, F. Yin, K. Kido, and S. Tsurekawa, "Electron-beam-induced c1urrent study of grain boundaries in multlcrystalline silicon," *Journal of Applied Physics*, vol. 96, no. 10, pp. 5490–5495, 2004.

[51] J. Chen and T. Sekiguchi, "Carrier recombination activity and structural properties of small-angle grain boundaries in multicrystalline silicon," *Japanese Journal of Applied Physics, Part 1*, vol. 46, no. 10, pp. 6489–6497, 2007.

[52] H. Sawada and H. Ichinose, "Structure of {112}Σ3 boundary in silicon and diamond," *Scripta Materialia*, vol. 44, no. 8-9, pp. 2327–2330, 2001.

[53] N. Sakaguchi, H. Ichinose, and S. Watanabe, "Atomic structure of faceted Σ3 CSL grain boundary in silicon: HRTEM and Ab-initio calculation," *Materials Transactions*, vol. 48, no. 10, pp. 2585–2589, 2007.

[54] N. Sakaguchi, M. Miyake, S. Watanabe, and H. Takahashi, "EELS and Ab-Initio study of faceted CSL boundary in

silicon," *Materials Transactions*, vol. 52, no. 3, pp. 276–279, 2011.

[55] P. Keblinski, S. R. Phillpot, D. Wolf, and H. Gleiter, "Thermodynamic criterion for the stability of amorphous intergranular films in covalent materials," *Physical Review Letters*, vol. 77, no. 14, pp. 2965–2968, 1996.

[56] M. Kohyama and R. Yamamoto, "Tight-binding study of grain boundaries in Si: energies and atomic structures of twist grain boundaries," *Physical Review B*, vol. 49, no. 24, pp. 17102–17117, 1994.

[57] S. Von Alfthan, P. D. Haynes, K. Kaski, and A. P. Sutton, "Are the structures of twist grain boundaries in silicon ordered at 0 K?" *Physical Review Letters*, vol. 96, no. 5, Article ID 055505, 2006.

[58] I. V. Markov, *Crystal Growth for Beginners*, World Scientific, Singapore, 1995.

[59] A. Voigt, E. Wolf, and H. P. Strunk, "Grain orientation and grain boundaries in cast multicrystalline silicon," *Materials Science and Engineering B*, vol. 54, no. 3, pp. 202–206, 1998.

[60] H. P. Iwata, U. Lindefelt, S. Öberg, and P. R. Briddon, "Energies and electronic properties of isolated and interacting twin boundaries in 3C-SiC, Si, and diamond," *Physical Review B*, vol. 68, no. 11, Article ID 113202, 2003.

[61] C. Raffy, J. Furthmüller, and F. Bechstedt, "Properties of hexagonal polytypes of group-IV elements from first-principles calculations," *Physical Review B*, vol. 66, no. 7, Article ID 075201, 2002.

[62] V. V. Voronkov, "Growth of a silicon crystal with one dislocation," *Kristallografiya*, vol. 20, no. 6, pp. 1145–1151, 1975.

[63] D. T. J. Hurle, "A mechanism for twin formation during Czochralski and encapsulated vertical Bridgman growth of III-V compound semiconductors," *Journal of Crystal Growth*, vol. 147, no. 3-4, pp. 239–250, 1995.

[64] K. Kutsukake, T. Abe, N. Usami, K. Fujiwara, K. Morishita, and K. Nakajima, "Formation mechanism of twin boundaries during crystal growth of silicon," *Scripta Materialia*, vol. 65, no. 6, pp. 556–559, 2011.

[65] E. Billig, "Growth of monocrystals of germanium from an undercooled melt," *Proceedings of the Royal Society of London Series A*, vol. 229, no. 1178, pp. 346–363, 1955.

[66] R. S. Wagner, "On the growth of germanium dendrites," *Acta Metallurgica*, vol. 8, no. 1, pp. 57–60, 1960.

[67] D. R. Hamilton and R. G. Seidensticker, "Propagation mechanism of germanium dendrites," *Journal of Applied Physics*, vol. 31, no. 7, pp. 1165–1168, 1960.

[68] K. K. Leung and H. W. Kui, "Microstructures of undercooled Si," *Journal of Applied Physics*, vol. 75, no. 2, pp. 1216–1218, 1994.

[69] K. Nagashio and K. Kuribayashi, "Growth mechanism of twin-related and twin-free facet Si dendrites," *Acta Materialia*, vol. 53, no. 10, pp. 3021–3029, 2005.

[70] R. Y. Wang, W. H. LI, and L. M. Hogan, "Faceted growth of silicon crystals in Al-Si alloys," *Metallurgical and Materials Transactions A*, vol. 28, no. 5, pp. 1233–1243, 1997.

[71] R. W. Cahn, "Twinned crystals," *Advances in Physics*, vol. 3, no. 12, pp. 363–445, 1954.

[72] M. Kitamura, N. Usami, T. Sugawara et al., "Growth of multicrystalline Si with controlled grain boundary configuration by the floating zone technique," *Journal of Crystal Growth*, vol. 280, no. 3-4, pp. 419–424, 2005.

[73] K. Fujiwara, H. Fukuda, N. Usami, K. Nakajima, and S. Uda, "Growth mechanism of the Si 110 faceted dendrite," *Physical Review B*, vol. 81, no. 22, Article ID 224106, 2010.

[74] K. Fujiwara, K. Maeda, N. Usami, and K. Nakajima, "Growth mechanism of Si-faceted dendrites," *Physical Review Letters*, vol. 101, no. 5, Article ID 055503, 2008.

[75] X. Yang, K. Fujiwara, R. Gotoh et al., "Effect of twin spacing on the growth velocity of Si faceted dendrites," *Applied Physics Letters*, vol. 97, no. 17, Article ID 172104, 2010.

[76] S. O'Hara and A. I. Bennett, "Web growth of semiconductors," *Journal of Applied Physics*, vol. 35, no. 3, pp. 686–693, 1964.

[77] D. L. Barrett, E. H. Myers, D.R. Hamilton, and A. I. Bennett, "Growth of wide, flat crystals of silicon web," *Journal of the Electrochemical Society*, vol. 118, no. 6, pp. 952–957, 1971.

[78] C. F. Lau and H. W. Kui, "Microstructures of undercooled germanium," *Acta Metallurgica Et Materialia*, vol. 39, no. 3, pp. 323–327, 1991.

[79] D. Li and D. M. Herlach, "Direct measurements of free crystal growth in deeply undercooled melts of semiconducting materials," *Physical Review Letters*, vol. 77, no. 9, pp. 1801–1804, 1996.

[80] T. Aoyama, Y. Takamura, and K. Kuribayashi, "Dendrite growth processes of silicon and germanium from highly undercooled melts," *Metallurgical and Materials Transactions A*, vol. 30, no. 5, pp. 1333–1339, 1999.

[81] X. Yang, K. Fujiwara, K. Maeda, J. Nozawa, H. Koizumi, and S. Uda, "Dependence of Si faceted dendrite growth velocity on undercooling," *Applied Physics Letters*, vol. 98, no. 1, Article ID 012113, 2011.

[82] I. Takahashi, N. Usami, K. Kutsukake, G. Stokkan, K. Morishita, and K. Nakajima, "Generation mechanism of dislocations during directional solidification of multicrystalline silicon using artificially designed seed," *Journal of Crystal Growth*, vol. 312, no. 7, pp. 897–901, 2010.

[83] N. Usami, R. Yokoyama, I. Takahashi, K. Kutsukake, K. Fujiwara, and K. Nakajima, "Relationship between grain boundary structures in Si multicrystals and generation of dislocations during crystal growth," *Journal of Applied Physics*, vol. 107, no. 1, Article ID 013511, 2010.

[84] V. Ganapati, S. Schoenfelder, S. Castellanos et al., "Infrared birefringence imaging of residual stress and bulk defects in multicrystalline silicon," *Journal of Applied Physics*, vol. 108, no. 6, Article ID 063528, 2010.

[85] G. Sarau, S. Christiansen, M. Holla, and W. Seifert, "Correlating internal stresses, electrical activity and defect structure on the micrometer scale in EFG silicon ribbons," *Solar Energy Materials and Solar Cells*, vol. 95, no. 8, pp. 2264–2271, 2011.

[86] S. Nakano, X. J. Chen, B. Gao, and K. Kakimoto, "Numerical analysis of cooling rate dependence on dislocation density in multicrystalline silicon for solar cells," *Journal of Crystal Growth*, vol. 318, no. 1, pp. 280–282, 2011.

[87] G. Stokkan, "Relationship between dislocation density and nucleation of multicrystalline silicon," *Acta Materialia*, vol. 58, no. 9, pp. 3223–3229, 2010.

[88] A. A. Istratov, T. Buonassisi, R. J. McDonald et al., "Metal content of multicrystalline silicon for solar cells and its impact on minority carrier diffusion length," *Journal of Applied Physics*, vol. 94, no. 10, pp. 6552–6559, 2003.

[89] B. Gao, S. Nakano, and K. Kakimoto, "Effect of crucible cover material on impurities of multicrystalline silicon in a unidirectional solidification furnace," *Journal of Crystal Growth*, vol. 318, no. 1, pp. 255–258, 2011.

[90] T. Buonassisi, A. A. Istratov, M. A. Marcus et al., "Engineering metal-impurity nanodefects for low-cost solar cells," *Nature Materials*, vol. 4, no. 9, pp. 676–679, 2005.

[91] G. Coletti, P. C.P. Bronsveld, G. Hahn et al., "Impact of metal contamination in silicon solar cells," *Advanced Functional Materials*, vol. 21, no. 5, pp. 879–890, 2011.

[92] P. Gundel, M. C. Schubert, W. Kwapil et al., "Micro-photoluminescence spectroscopy on metal precipitates in silicon," *Physica Status Solidi—Rapid Research Letters*, vol. 3, no. 7-8, pp. 230–232, 2009.

[93] T. Buonassisi, A. A. Istratov, M. D. Pickett et al., "Micro-photoluminescence spectroscopy on metal precipitates in silicon," *Progress in Photovoltaics*, vol. 14, no. 6, pp. 513–531, 2006.